ACS OMEGA

Open Access

http://pubs.acs.org/journal/acsodf

Article

Advanced Molecular Dynamics Model for Investigating Biological-Origin Microfibril Structures

Veerapandian Ponnuchamy,* Anna Sandak, and Jakub Sandak

Cite This: *ACS Omega* 2024, 9, 25646−25654

Read Online

ACCESS | Metrics & More | Article Recommendations | Supporting Information

ABSTRACT: Understanding the atomic-scale structure of wood microfibrils is essential for establishing fundamental properties in various wood-based research aspects, including moisture impact, wood modification, and pretreatment. In this study, we employed molecular dynamics simulations to investigate the arrangement of wood polymers, including cellulose, hemicellulose, and lignin, with a primary focus on the composition of softwood, specifically Norway Spruce wood. We assessed the accuracy of our molecular dynamics model by comparing it with available experimental data, such as density, Young's modulus, and glass transition temperature, which ensures the reliability of our approach. A key aspect of our study involved modeling the active sorption site for water interaction with wood polymers. Our findings revealed that the interaction between water and hemicellulose, particularly within the hemicellulose−cellulose interphase, was the most prominent binding site. This observation aligns with prior research in this field, further strengthening the validity of our results.

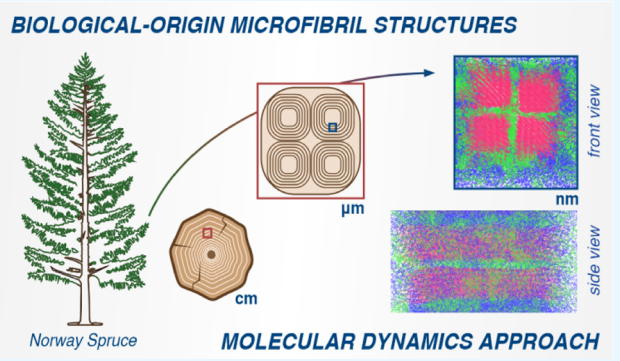

1. INTRODUCTION

Wood is a renewable and versatile material used for different types of load-bearing structures as well as complementary constructive components, such as cladding, decking, doors, and windows. Its cell wall is composed of primary and secondary walls, with the latter being multilayered (Figure 1). At a microscopic level, the secondary wall is made up of three layers (S1, S2, and S3), with the S2 layer contributing to approximately 80% of the cell volume.[1] The major polymers in the cell wall are cellulose, hemicellulose, and lignin, bound together as a fiber-reinforced composite that imparts mechanical strength to wood. The specific composition of polymers greatly differs based on plant origin, genetic configuration, silvicultural activities, and location, leading to variations in microfibril dimensions, proportions, and alignments. The arrangement of polymers on the microscopic scale is organized as follows. Cellulose is a carbohydrate-based polymer formed in a crystalline (or semicrystalline) phase and located in the central core of the fibril, while amorphous polymers, including hemicellulose and lignin, are situated in the middle and outermost layer, respectively.[2]

The arrangement of cellulose fibrils causes the anisotropic nature of the microfibril, where the longitudinal elastic and strength properties exceed those in the transverse direction.[3,4] Additionally, wood shows a strong inclination to absorb water from the environment, leading to significant alterations in its properties such as dimensional changes and a decrease in elastic properties.[5−7] A comprehensive review by Engelund et al.[8] provides detailed context on the interaction between wood and water. This review explained that water molecules tend to bind hemicellulose strongly, followed by cellulose and lignin. Several studies using experimental and numerical methods have attempted to quantify the diffusion mechanism of water. Thybring et al. showed that the oven-dried samples exhibited lower hydroxyl accessibility as hemicellulose undergoes degradation. This demonstrated that the hydroxyl groups in hemicellulose are the more pronounced site for water sorption during moisture influence.[9] Experimental findings using small-angle neutron scattering and hydrogen/deuterium methods show that hydroxyl groups in cellulose and hemicellulose are the primary interaction sites for moisture absorption.[10−13] Similar results have been observed with atomistic modeling investigations.[14−16] Despite several studies on moisture absorption in wood, the underlying mechanism of this process is still under debate. The atomistic modeling methods can support and provide an understanding of the anisotropic swelling observed in experiments. The scientific community is still debating several other cell wall properties, including electric conductivity, resistance against biotic and abiotic deteriorations, and molecular mechanisms of chemical and

Received: November 7, 2023
Revised: April 28, 2024
Accepted: May 21, 2024
Published: June 6, 2024

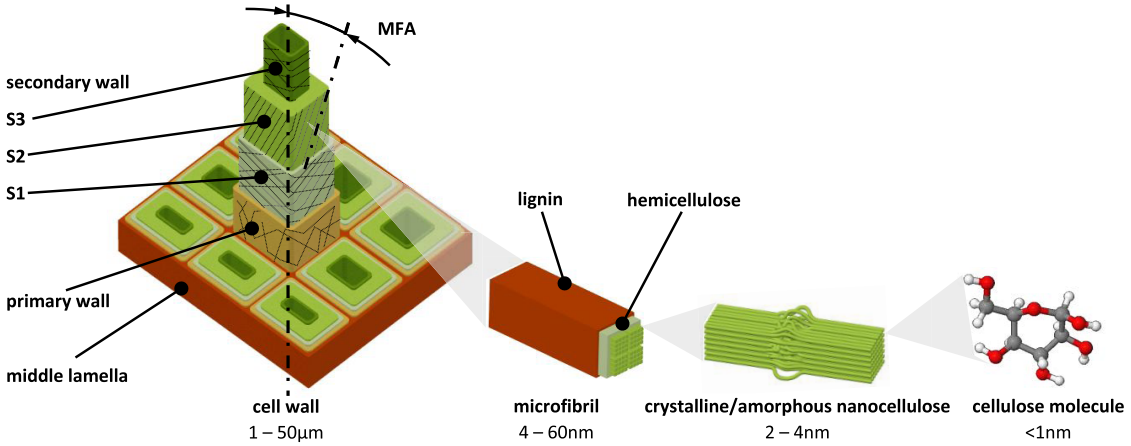

Figure 1. Hierarchical structure of wood from molecule to the cell wall levels.

physical material modifications. Molecular dynamics (MD) simulations can provide an in-depth understanding of material behavior at the atomic scale, and therefore, this method is essential for studying the polymers present in the wood fibril.[15,17,18]

The Derome group has established multiple models to study cellulose, hemicellulose, and lignin using atomic modeling and has contributed to the understanding of the hysteric behavior of individual wood polymers and the S2 layer.[15,19−26] One of their works designed the S2 layer to investigate the influence of moisture content using molecular dynamics (MD) simulations.[15] They illustrated the properties of the S2 layer under dry and moisture conditions and compared them with experimental results. However, the proposed model has some shortcomings, such as uncertainty of mechanical modulus, lack of information on the distribution of the lignin structure model, inadequate information on the lignin force field (GROMOS 53a6 force field) used for the MD simulations, insufficient details on the sorption site of water, and unavailability of the model for replication or direct use in research. Furthermore, a recent work investigates the complex composition of plant secondary cell walls (SCWs) using solid-state nuclear magnetic resonance (ssNMR).[27] The study refines our understanding of the intermolecular interactions and higher-order architecture of cellulose, hemicelluloses, and lignin within air-dried Populus wood. Molecular dynamics simulations further validate these structural insights, emphasizing the integration of experimental and computational approaches.

Here, we focus on the preparation of atomistic representation of microfibril, considering the composition of softwood, Norway spruce. The microfibril is constructed from the fundamental units of wood polymers such as cellulose (CC), hemicellulose (HC), and lignin (LIG) that are present in softwood. After MD simulations, density, Young's modulus, and glass transition temperature are extracted and compared with experiments. Another objective of this work is to find out the key sorption site of interaction water in the wood microfibril, in which additional MD simulations are carried out by placing water molecules in the entire fibril. The final results obtained from water interaction with wood polymers are given by calculating the mean square displacement, diffusion coefficient, and hydrogen-bonding analyses.

2. METHODS

2.1. Molecular Dynamics Simulations: Preparation of Microfibril. Here, we briefly demonstrate different state-of-the-art tools and techniques integrated to assemble an advanced MD model of a wood microfibril. The core of the fibril was built by four crystalline cellulose (CC) matrices organized in a square format. The CC was constructed using the cellulose-builder toolkit proposed by Gomes et al.[28] Each single cellulose polymer chain is composed of 40 repeating glucose units (degree of polymerization = 40), and a single CC is formed by 36 chains. In the case of hemicellulose (HC), galatoglucomannan (GGM) was used for simulations, as GGM is the dominant chemical structure present in softwood. The chosen GGM was formed by the combination of glucose, mannose, and galactose, and 16 units with 5 branches were created. CHARMM-GUI was used to make the GGM model.[29] The native structure of lignin is highly heterogeneous. Therefore, a softwood-based lignin model with a molecular weight of 1.2 kDa was developed for the needs of this study.[30,31] An integrated approach was employed to build the lignin structure by combining different tools, such as LigninBuilder,[32] TopoGromacs,[33] and TopoTools.[34] All inter- and intramolecular interactions are accounted by the CHARMM force field potential[35,36] as this CHARMM force field is able to reproduce the experimental results.[37−39] The cutoff at 1.2 nm was used for nonbonded interactions, particle-mesh Ewald summation (PME) was applied for long-range electrostatic interactions, and the covalently bonded hydrogens were constrained using LINCS during all simulations. All MD simulations are carried out using GROMACS[40] with a CUDA-GPU-supported package.

Several steps were employed: (i) energy minimization was performed using steepest decent followed by conjugate gradient methods, (ii) equilibration with NVT ensemble was applied for 5 ns at 300 K, followed by (iii) employing NPT ensemble with 400 K and 500 MPa stress for 5 ns; CC structures were constrained to maintain the crystallinity in this step, (iv) annealing the temperature from 400 to 300 K was done at 10 K/ps with 0.1 MPa (or 1 bar), and (v) the final production run was carried out at NPT condition with 300 K and 1 bar for 300 ns, in which the last 50 ns was used for the analysis. The convergence of the trajectory is shown in the Supporting Information. A constant strain rate of 5×10^8 s^{-1} was applied in a given axis under NPT conditions for Young's modulus calculation. The initial 4% stress−strain curve was

https://doi.org/10.1021/acsomega.3c08853
ACS Omega 2024, 9, 25646−25654

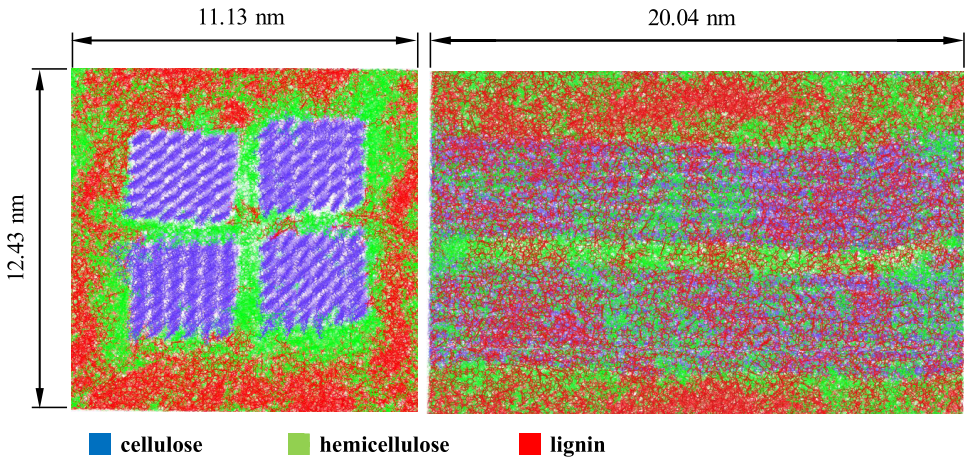

Figure 2. Molecular dynamics model of Norway spruce fibril. Note: dimensions correspond to the simulation model box.

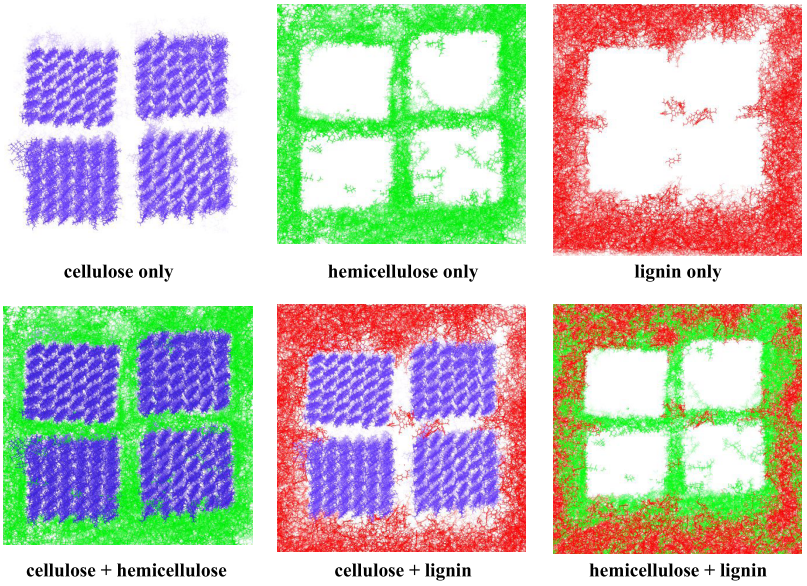

Figure 3. Distribution and interactions of cellulose, hemicellulose, and lignin within the MD model of Norway spruce fibril.

fitted as a linear function. The slope of the line was assumed as Young's modulus E value. The glass transition temperature was calculated by increasing the temperature from 300 to 600 K after the NPT production run and followed by cooling the box from 600 to 0 at 0.1 K/ps to calculate glass transition temperature (T_g).

2.2. Water Interaction with the Microfibril. To investigate the interaction between water and wood polymers, we introduced a water molecule into the microfibril using 1000 distinct configurations, ensuring that each polymer component was considered without duplication of the same position or orientation. Notably, the cellulose crystalline units within the fibril remained intact, and the resulting configurations with water molecules randomly placed confirmed the absence of water penetration in the crystalline regions of cellulose. After 200 ps of simulations conducted under NVT conditions, we calculated the potential energy for all 1000 configurations and compared them. From this analysis, we selected the final two configurations based on their stability, specifically choosing those with the lowest energy among all examined configurations and the most favorable water placement. The selected configurations were then subjected to a series of steps, including minimization, equilibration, and a production run lasting 25 ns, all of which were performed using the same simulation setup as described above. The TIP3P model was considered in the present study for water, and the CHARMM potential was used for inter- and intramolecular interactions.[41]

3. RESULTS AND DISCUSSION

3.1. Validation of Dry Microfibril. The spatial distribution of these molecules after the proprietary model arrangement is presented in Figure 2, where each polymer is differentiated by color. The total volume of the model box was 2819.0 nm^3. The chemical nature of these polymers promotes the bonding of hemicellulose with both cellulose and lignin. The direct interaction of cellulose and hemicellulose was substantially higher, about an average of five times, than that of cellulose−lignin. This was confirmed as shown in Figure 3, where the distribution of the separate components, as well as the pairs, are presented. The proposed MD model interactions were consistent with the previous findings, in which the authors employed solid-state NMRs and computational modeling to account for the detailed structural characteristics of plant cell walls.[42−45]

https://doi.org/10.1021/acsomega.3c08853
ACS Omega 2024, 9, 25646−25654

The wood fibril model was validated against important properties such as the density of wood in a dry state, Young's modulus of elasticity, and glass transition temperature. Our model is superior compared to those previously proposed in the literature because of the transparency in the force fields, a more rational lignin structure and distribution, and openly available data for the recreation of the softwood fibril model. We have considered Norway spruce (*Pica abies*) softwood as a natural biomaterial reference to create a corresponding fibril model. The composition of the predominant polymers such as cellulose, hemicellulose, and lignin is presented in Table 1.[46]

Table 1. Composition of the Constructed Fibril Model for Softwood Based on the Existing Composition of Softwood

chemical components	cellulose	hemicellulose	lignin	total
Norway spruce wood				
mass ratio % for MD model	42	30	28	100
the molecular weight of a polymer chain	6488	3422	1161	11,071
no. of polymer chains	36 × 4	196	536	846
atoms	121,392	87,024	81,472	289,888

Three key properties of the fibril were calculated based on this atomistic model, including bulk density ρ, Young's modulus of elasticity E, and glass transition temperature T_g. In Table 2, values obtained by numerical simulation are compared to the corresponding data available in the literature.

The resulting density of the fibril simulated with the MD model was 1338 kg m^{-3}, which is in agreement with the value predicted using the alternative MD model (1352 kg m^{-3}), as reported by Kulasinski et al.[15] The simulated density values closely correspond to the experimental data summarized in Table 2.[47,48] In that case, the bulk density of Norway spruce, determined experimentally, varied in the range of 1500−1529 kg m^{-3}. Additionally, we computed the density of individual polymer components to evaluate the force field and found that crystalline cellulose, hemicellulose, and lignin exhibited 1460, 1361, and 1202 kg m^{-3}, respectively. Considering these densities from the CHARMM force field, the overall fibril density could be influenced by accumulated errors from each component. The average values of hemicellulose and lignin densities combined are approximately 1281 kg m^{-3}. This may significantly impact the overall density of our system, particularly when combined with the observed crystalline cellulose density of ∼1460 kg m^{-3} in the fibril.

Young's modulus E was calculated in three anisotropy directions (x, y, and z) as the microfibril's properties are orthotropic. Therefore, the modulus in the z-direction was defined as longitudinal, while other axes (x and y) were transverse. The simulated Young's modulus values in both transverse directions resulted in comparable values of 4.4 and 4.1 GPa for the x and y axis, respectively. These results align with the values proposed by alternative MD simulations[15] as well as experimental works.[49] The arrangement of the crystalline cellulose chain within the fibril in the x and y directions is rather similar and in the same dimensional order. Conversely, it is rather difficult to directly compare Young's modulus in the longitudinal (z) direction determined in MD simulations with the values reported in the literature. The main reason is due to the great variation of E with respect to the microfibril angle. In such instances, various authors[49−51] reported Young's modulus results as a function of the microfibril angle. These ranged from 10 to 70 GPa for transverse (90°) and longitudinal directions (0°), respectively. The E value in the z-axis direction determined through the presented MD model was 22.1 GPa, falling within the range of references. It is important to highlight that direct comparisons between macroscopic values of wood fibril and MD fibril-derived values may pose challenges. This is attributed to variations in the molecular arrangement, porosity distribution, and the varying crystallinity levels observed in cellulose.

The glass transition temperature was calculated based on the density fitting method, as presented by Lin et al.[52] The MD fibril model presented here predicts the T_g value of 401.7 K after fitting the density values from 600.0 to 0.0 K. It is within the range of 333.2 to 473.2 K as reported in the literature for wood fibrils. The relatively broad range of wood T_g is related to the diversity of wood due to species as well as the variations induced by geographical origin and silviculture. Moreover, the T_g values of amorphous polymers such as hemicellulose and lignin were also calculated separately to understand their impact on the overall T_g value. It is evident that the T_g of lignin (∼409.0 K) contributes heavily to the T_g of the fibril, as this temperature is close to that of the whole fibril complex simulated with MD. Conversely, the T_g of hemicellulose (∼356 K) was smaller. This is consistent with state-of-the-art knowledge and further supported by the experiments. It is commonly assumed that the T_g of wood corresponds to the T_g of the lignin constituting wood.[53,54]

3.2. Water Interaction with the Microfibril. It is essential to emphasize that our proposed model lacks the presence of water, which hinders the elucidation of the

Table 2. Fibril Properties Simulated with the Presented MD Model in Comparison with Alternative MD Models and Experimental Values Reported in Literature References[c]

property	parameters	this study	exp
bulk density, ρ (kg m^{-3})		1338.00 (1.73)[a]	1500[47]
			1517−1529[48]
Young's modulus of elasticity, E (GPa)	X	4.44	4.3−4.6[b49]
	Y	4.06	4.3−4.6[b49]
	Z (longitudinal)	22.07	21−37[b49]
glass transition temperature, T_g (K)	fibril	404.47	333.15−473.15[53,54]
	hemicellulose	356.00	313.15[53,54]
	lignin	409.09	323.15−373.15[24]

[a]Standard deviation is mentioned in the parentheses. [b]The range of Young's modulus in the longitudinal direction was calculated based on the cellulose microfibril angle. [c]Young's modulus values were measured for different Spruce wood species.

https://doi.org/10.1021/acsomega.3c08853
ACS Omega 2024, 9, 25646−25654

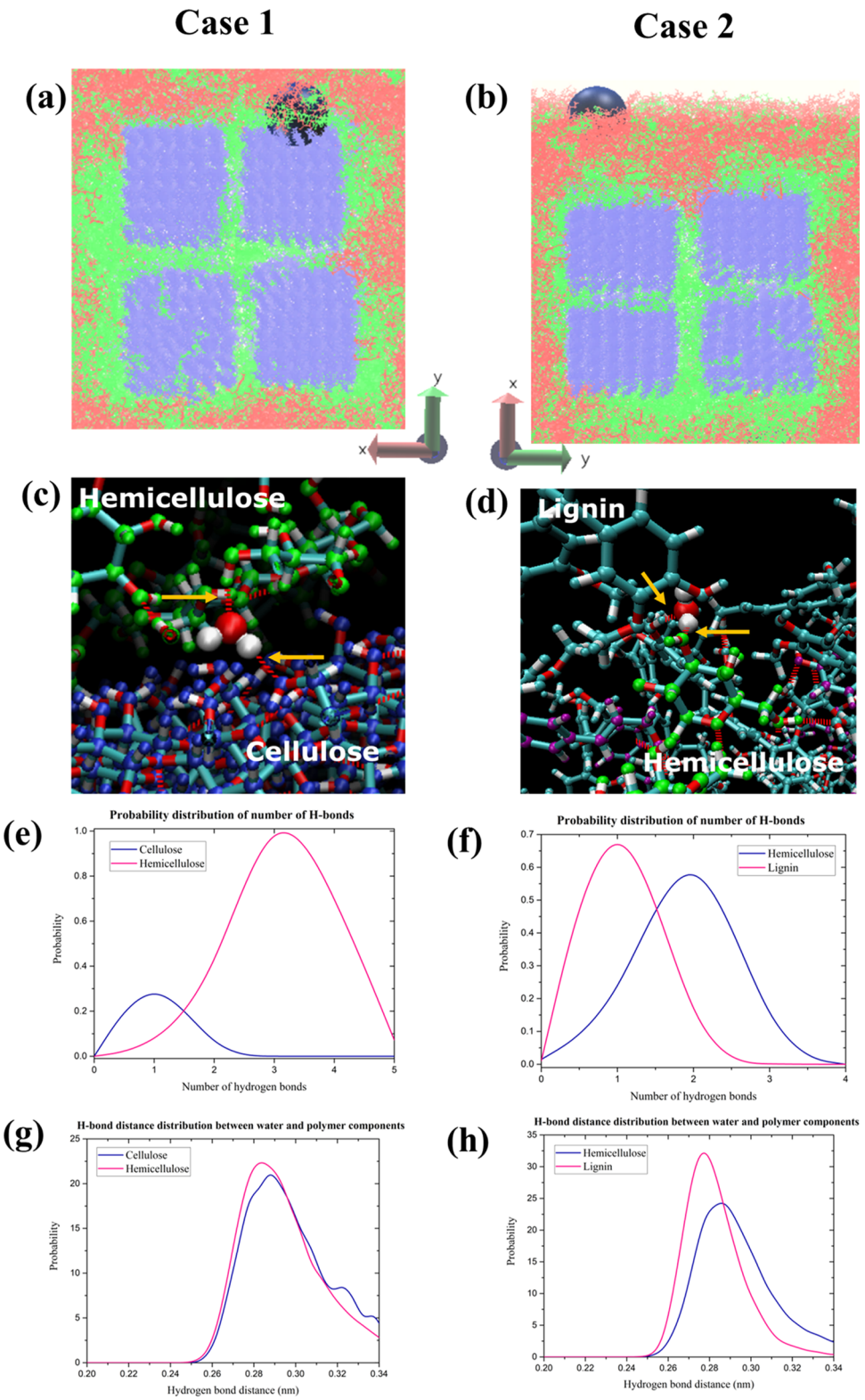

Figure 4. (a, b) Chosen configurations of water in the fibril with respect to different positions (cases 1 and 2); the blue color bead in each represents the location of water in the fibril matrix. (c, d) Specific location of water interacting with fibril components; arrows indicate the hydrogen bonds. (e, f) Probability distribution of the number of hydrogen bonds existing between cellulose−hemicellulose for case 1, hemicellulose−lignin for case 2. (g, h) Typical hydrogen bond distance between and fibril components.

moisture influence mechanism.[55,56] Several experimental studies have proposed that water tends to bind to different active sites, corresponding to lignin and carbohydrate polymers. Predicting such behavior is challenging with existing techniques due to the complex arrangement of the polymer matrix in wood.[57,58] The binding mechanism remains a subject of debate, with no concrete description of water-absorbing sites in dry wood available to date. In this study, we aimed to shed

https://doi.org/10.1021/acsomega.3c08853
ACS Omega 2024, 9, 25646−25654

light on the underlying mechanism of fundamental water-binding sites in dry wood by randomly placing water molecules within the polymer matrix.

After performing comprehensive simulations by randomly placing the water in the fibril, we observed two distinct configurations of water interaction with wood components. For instance, we observed water located at the interphase between crystalline cellulose and hemicellulose, as well as another configuration where water is present in the amorphous polymer region interphase (hemicellulose and lignin). These configurations are illustrated in Figure 4, and a few properties of the fibril-water are presented in Table 3. Subsequent simulations, including minimization, equilibration, and production runs lasting 25 ns, were carried out using the most stable configurations.

Table 3. Relative Potential Energy, Volume, Density, and Diffusion Coefficient of Water from Two Chosen Configurations, Containing Fibril and Water[a]

properties	case 1	case 2
relative potential energy (kJ mol^{-1})	0	1110
volume (nm^3)	2812.57 (±1.59)	2814.83 (±1.50)
density (kg m^{-3})	1316.51 (±0.76)	1315.46 (±0.70)
diffusion coefficient of water ($1e^{-9}$ cm^2 s^{-1})	1.035	0.847

[a]The standard deviation is mentioned in the parentheses.

Notably, our results indicate that water binding at the interphase between crystalline cellulose and hemicellulose (case 1) exhibited a higher potential energy compared to water presented in the hemicellulose−lignin regions (case 2), with an associated energy difference of approximately 1110 kJ/mol. A similar trend was observed in the mean square displacement (MSD) results, where case 1 demonstrated higher MSD and diffusivity than case 2 (from Table 3). Several factors may contribute to this difference, including weaker binding or interaction between water and the cellulose−hemicellulose matrix in case 1. Furthermore, variations in pore size at the distinct phase between cellulose−hemicellulose (crystalline−amorphous) may result in less confinement of water compared to the amorphous hemicellulose−lignin network (case 2), as the pore networks are significantly smaller in amorphous polymers than in case 1. Additionally, the hydrophilic nature of the cellulose surface and hemicellulose may impact water-attracting properties and result in weaker polymer−water interactions, ultimately leading to higher water mobility.

We further explored these results by analyzing the hydrogen bond network between water and the polymer matrix. In case 1, the number of hydrogen bonds is significantly dominated by hemicellulose, with approximately three hydrogen bonds formed compared to one hydrogen bond for cellulose. The probability of hydrogen bond formation is also twice as high for hemicellulose compared to cellulose. Similarly, in case 2, hemicellulose again dominated the number of hydrogen bonds, with two in total compared to one for lignin. However, the probability of hydrogen bond formation with lignin is slightly higher than that with hemicellulose, despite the lower number of hydrogen bonds. These results correlate with the lifetime of hydrogen bonds calculated for both cases. In case 1, the hydrogen bond lifetime for cellulose with water is 2.67 ps, which is lower than that for hemicellulose with water (5.71 ps). Conversely, in case 2, lignin significantly dominates the hydrogen bond lifetime, with a value of approximately 121.73 ps, compared to hemicellulose with 8.58 ps. Overall, our findings emphasize that hemicellulose dominates the water interaction in case 1, while lignin plays a predominant role in hydrogen bonding in case 2. The simulation results are in good agreement with the experimental findings proposed earlier that hemicellulose is the more pronounced site to adsorb water during water dynamics, compared to cellulose and lignin.[8,59] In both cases 1 and 2, hemicellulose plays a critical role in water dynamics due to the fact of hydrophilic characteristics, while lignin exhibits a lower interaction with water because of its aromatic hydrophobic structure.

In summary, the proposed MD model of the fibril and its configuration are adequate to represent wood fibrils at the atomic scale. Although this fundamental solution corresponds to the smallest wood constituent unit, some percentage of error in the prediction of the proposed properties cannot be prevented. The source of error can be associated with the three following factors. First, the representation of the force field parameters is limited due to the large number of atoms representing the different constituents of the fibril. Second, the genuine molecular models of amorphous polymers, hemicellulose, and lignin are limited due to the heterogeneity of biological-origin materials. A relatively small size of the hemicellulose and lignin molecules was used in the model. Nevertheless, the structural distribution and composition of these chains are heterogeneous, leading to a good analogy to natural systems. It is particularly relevant to the lignin polymeric structure represented here in such a complex configuration for the first time. Finally, the numeric system preparation is identified as a third source of error. The protocol developed for the generation of the fibril model involves several steps that are indispensable to achieving the most realistic fibril structure representation that is possible. The MD simulations especially influence the misrepresentation of the fibril properties due to the distinct distribution of molecules in the box. It should be mentioned that the accepted error range for describing material properties is smallest at the macroscopic scale due to the possibility of more uniform homogenization of the polymers. Conversely, as the scale of the system is reduced, the minor changes in the distribution of molecules may significantly impact the estimated materials' properties, leading to the higher expected and tolerated inaccuracy.

4. CONCLUSIONS

Molecular dynamics simulations were employed to develop a fundamental microfibril system at the atomic scale. Such a model is a fundamental prerequisite for any research involving wood and lignocellulosic biomass. This study concentrates on creating a microfibril model using Norway Spruce wood as the basis. Several properties, including density, Young's modulus, and the glass transition temperature obtained from these simulations, are validated against experimental values. The results demonstrate excellent agreement with the existing literature. To investigate water interactions with wood components, a water molecule was randomly placed within the matrix, generating around a thousand different configurations. From these, two of the most stable configurations were selected for a detailed study of the water dynamics. The findings reveal that hemicellulose is the dominant component

https://doi.org/10.1021/acsomega.3c08853
ACS Omega 2024, 9, 25646−25654

in water interactions. Particularly, the cellulose−hemicellulose interphase exhibits more pronounced water dynamics compared to those of the hemicellulose−lignin interphase. This insight provides a deeper understanding of water interactions with fibril components, further clarifying the experimental objectives. This microfibril model serves as a crucial precursor for wood-based research, encompassing the simulation of biological processes, biorefinery, modification, functionalization, chemical, mechanical, and enzymatic pretreatment processes, solvent-based fractionation, wood-based composites, and more. Importantly, we emphasize that the step-by-step protocol of this proposed model preparation, along with troubleshooting, will be published soon under the name of the same authors as an open source and will be freely available.

■ ASSOCIATED CONTENT

Data Availability Statement

The data underlying this study are openly available on zenodo.org at 10.5281/zenodo.11079249.

Supporting Information

The Supporting Information is available free of charge at https://pubs.acs.org/doi/10.1021/acsomega.3c08853.

Convergence plot time (ns) vs volume (nm^3) of the fibril (PDF)

All input (.pdb, .gro) and force field files (.itp) for the fibril (ZIP)

■ AUTHOR INFORMATION

Corresponding Author

Veerapandian Ponnuchamy − *InnoRenew CoE, 6310 Izola, Slovenia; University of Primorska, Andrej Marušič Institute, 6000 Koper, Slovenia;* Present Address: Department of Mechanical Engineering, Eindhoven University of Technology, 5600 MB Eindhoven, The Netherlands, v.ponnuchamy@tue.nl; orcid.org/0000-0002-7702-1462; Email: veerapandian.ponnuchamy@innorenew.eu

Authors

Anna Sandak − *InnoRenew CoE, 6310 Izola, Slovenia; University of Primorska, Andrej Marušič Institute, 6000 Koper, Slovenia; Faculty of Mathematics, Natural Sciences and Information Technologies, University of Primorska, 6000 Koper, Slovenia*

Jakub Sandak − *InnoRenew CoE, 6310 Izola, Slovenia; University of Primorska, Andrej Marušič Institute, 6000 Koper, Slovenia*

Complete contact information is available at: https://pubs.acs.org/10.1021/acsomega.3c08853

Notes

The authors declare no competing financial interest.

■ ACKNOWLEDGMENTS

The authors gratefully acknowledge the European Commission for funding the InnoRenew project [Grant Agreement #739574] under the Horizon2020 Widespread-Teaming program, the Republic of Slovenia (investment funding of the Republic of Slovenia and the European Union European Regional Development Fund) and infrastructural ARRS program IO-0035. Part of this work was conducted during project HYGRO-WOOD (BI-LT/20-22-002) funded by ARRS. A.S. would like to thank the Horizon Europe−European Research Council Consolidator Grant under ARCHI-SKIN (Grant Number #101044468). Views and opinions expressed are however those of the author(s) only and do not necessarily reflect those of the European Union or the European Research Council Executive Agency. Neither the European Union nor the granting authority can be held responsible for them.

■ REFERENCES

(1) Salmén, L. Micromechanical Understanding of the Cell-Wall Structure. *C. R. Biol.* **2004**, *327* (9), 873−880.

(2) Qing, H.; Mishnaevsky, L. 3D Hierarchical Computational Model of Wood as a Cellular Material with Fibril Reinforced, Heterogeneous Multiple Layers. *Mech. Mater.* **2009**, *41* (9), 1034−1049.

(3) Salmén, L. Wood Morphology and Properties from Molecular Perspectives. *Ann. For. Sci.* **2015**, *72* (6), 679−684.

(4) Mani, S.; Cosgrove, D. J.; Voth, G. A. Anisotropic Motions of Fibrils Dictated by Their Orientations in the Lamella: A Coarse-Grained Model of a Plant Cell Wall. *J. Phys. Chem. B* **2020**, *124* (17), 3527−3539.

(5) Derome, D.; Rafsanjani, A.; Patera, A.; Guyer, R.; Carmeliet, J. Hygromorphic Behaviour of Cellular Material: Hysteretic Swelling and Shrinkage of Wood Probed by Phase Contrast X-Ray Tomography. *Philos. Mag.* **2012**, *92* (28−30), 3680−3698.

(6) Patera, A.; Derome, D.; Griffa, M.; Carmeliet, J. Hysteresis in Swelling and in Sorption of Wood Tissue. *J. Struct. Biol.* **2013**, *182* (3), 226−234.

(7) Etale, A.; Onyianta, A. J.; Turner, S. R.; Eichhorn, S. J. Cellulose: A Review of Water Interactions, Applications in Composites, and Water Treatment. *Chem. Rev.* **2023**, *123* (5), 2016−2048.

(8) Engelund, E. T.; Thygesen, L. G.; Svensson, S.; Hill, C. A. S. A Critical Discussion of the Physics of Wood−Water Interactions. *Wood Sci. Technol.* **2013**, *47* (1), 141−161.

(9) Thybring, E. E.; Thygesen, L. G.; Burgert, I. Hydroxyl Accessibility in Wood Cell Walls as Affected by Drying and Re-Wetting Procedures. *Cellulose* **2017**, *24* (6), 2375−2384.

(10) Willems, W. Hygroscopic Wood Moisture: Single and Dimerized Water Molecules at Hydroxyl-Pair Sites? *Wood Sci. Technol.* **2018**, *52* (3), 777−791.

(11) Rautkari, L.; Hill, C. A. S.; Curling, S.; Jalaludin, Z.; Ormondroyd, G. What Is the Role of the Accessibility of Wood Hydroxyl Groups in Controlling Moisture Content? *J. Mater. Sci.* **2013**, *48* (18), 6352−6356.

(12) Beck, G.; Strohbusch, S.; Larnøy, E.; Militz, H.; Hill, C. Accessibility of Hydroxyl Groups in Anhydride Modified Wood as Measured by Deuterium Exchange and Saponification. *Holzforschung* **2017**, *72* (1), 17−23.

(13) O'Neill, H.; Pingali, S. V.; Petridis, L.; He, J.; Mamontov, E.; Hong, L.; Urban, V.; Evans, B.; Langan, P.; Smith, J. C.; Davison, B. H. Dynamics of Water Bound to Crystalline Cellulose. *Sci. Rep.* **2017**, *7* (1), No. 11840.

(14) Kulasinski, K.; Guyer, R.; Derome, D.; Carmeliet, J. Water Diffusion in Amorphous Hydrophilic Systems: A Stop and Go Process. *Langmuir* **2015**, *31* (39), 10843−10849.

(15) Kulasinski, K.; Derome, D.; Carmeliet, J. Impact of Hydration on the Micromechanical Properties of the Polymer Composite Structure of Wood Investigated with Atomistic Simulations. *J. Mech. Phys. Solids* **2017**, *103*, 221−235.

(16) Bertinetti, L.; Fratzl, P.; Zemb, T. Chemical, Colloidal and Mechanical Contributions to the State of Water in Wood Cell Walls. *New J. Phys.* **2016**, *18* (8), No. 083048.

(17) Sarkar, D.; Bu, L.; Jakes, J. E.; Zieba, J. K.; Kaufman, I. D.; Crowley, M. F.; Ciesielski, P. N.; Vermaas, J. V. Diffusion in Intact Secondary Cell Wall Models of Plants at Different Equilibrium Moisture Content. *Cell Surf.* **2023**, *9*, No. 100105.

(18) Ponnuchamy, V. Multiscale Modeling Studies for Exploring Lignocellulosic Biomass Structure. In *Advanced Catalysis for Drop-in Chemicals*; Sudarsanam, P.; Li, H., Eds.; Elsevier, 2022; pp 257−289.
(19) Chen, M.; Zhang, C.; Shomali, A.; Coasne, B.; Carmeliet, J.; Derome, D. Wood−Moisture Relationships Studied with Molecular Simulations: Methodological Guidelines. *Forests* **2019**, *10* (8), No. 628.
(20) Derome, D.; Kulasinski, K.; Zhang, C.; Chen, M.; Carmeliet, J. Using Modeling to Understand the Hygromechanical and Hysteretic Behavior of the S2 Cell Wall Layer of Wood. In *Plant Biomechanics: From Structure to Function at Multiple Scales*; Geitmann, A.; Gril, J., Eds.; Springer International Publishing: Cham, 2018; pp 247−269.
(21) Zhang, C.; Chen, M.; Coasne, B.; Keten, S.; Derome, D.; Carmeliet, J. Hygromechanics of Softwood Cellulosic Nanocomposite with Intermolecular Interactions at Fiber-Matrix Interface Investigated with Molecular Dynamics. *Composites, Part B* **2022**, *228*, No. 109449.
(22) Kulasinski, K.; Keten, S.; Churakov, S. V.; Derome, D.; Carmeliet, J. A Comparative Molecular Dynamics Study of Crystalline, Paracrystalline and Amorphous States of Cellulose. *Cellulose* **2014**, *21* (3), 1103−1116.
(23) Chen, M.; Coasne, B.; Derome, D.; Carmeliet, J. Coupling of Sorption and Deformation in Soft Nanoporous Polymers: Molecular Simulation and Poromechanics. *J. Mech. Phys. Solids* **2020**, *137*, No. 103830.
(24) Kulasinski, K.; Guyer, R.; Derome, D.; Carmeliet, J. Water Adsorption in Wood Microfibril-Hemicellulose System: Role of the Crystalline−Amorphous Interface. *Biomacromolecules* **2015**, *16* (9), 2972−2978.
(25) Kulasinski, K.; Guyer, R.; Keten, S.; Derome, D.; Carmeliet, J. Impact of Moisture Adsorption on Structure and Physical Properties of Amorphous Biopolymers. *Macromolecules* **2015**, *48* (8), 2793−2800.
(26) Kulasinski, K.; Keten, S.; Churakov, S. V.; Guyer, R.; Carmeliet, J.; Derome, D. Molecular Mechanism of Moisture-Induced Transition in Amorphous Cellulose. *ACS Macro Lett.* **2014**, *3* (10), 1037−1040.
(27) Addison, B.; Bu, L.; Bharadwaj, V.; Crowley, M. F.; Harman-Ware, A. E.; Crowley, M. F.; Bomble, Y. J.; Ciesielski, P. N. Atomistic, Macromolecular Model of the Populus Secondary Cell Wall Informed by Solid-State NMR. *Sci. Adv.* **2024**, *10* (1), No. eadi7965.
(28) Gomes, T. C. F.; Skaf, M. S. Cellulose-Builder: A Toolkit for Building Crystalline Structures of Cellulose. *J. Comput. Chem.* **2012**, *33* (14), 1338−1346.
(29) Jo, S.; Kim, T.; Iyer, V. G.; Im, W. CHARMM-GUI: A Web-Based Graphical User Interface for CHARMM. *J. Comput. Chem.* **2008**, *29* (11), 1859−1865.
(30) Sumer, Z.; Van Lehn, R. C. Heuristic Computational Model for Predicting Lignin Solubility in Tailored Organic Solvents. *ACS Sustainable Chem. Eng.* **2023**, *11* (1), 187−198.
(31) Jahan, N.; Huda, M. M.; Tran, Q. X.; Rai, N. Effect of Solvent Quality on Structure and Dynamics of Lignin in Solution. *J. Phys. Chem. B* **2022**, *126* (31), 5752−5764.
(32) Vermaas, J. V.; Dellon, L. D.; Broadbelt, L. J.; Beckham, G. T.; Crowley, M. F. Automated Transformation of Lignin Topologies into Atomic Structures with LigninBuilder. *ACS Sustainable Chem. Eng.* **2019**, *7* (3), 3443−3453.
(33) Vermaas, J. V.; Hardy, D. J.; Stone, J. E.; Tajkhorshid, E.; Kohlmeyer, A. TopoGromacs: Automated Topology Conversion from CHARMM to GROMACS within VMD. *J. Chem. Inf. Model.* **2016**, *56* (6), 1112−1116.
(34) Humphrey, W.; Dalke, A.; Schulten, K. VMD: Visual Molecular Dynamics. *J. Mol. Graphics* **1996**, *14* (1), 33−38.
(35) Vanommeslaeghe, K.; Hatcher, E.; Acharya, C.; Kundu, S.; Zhong, S.; Shim, J.; Darian, E.; Guvench, O.; Lopes, P.; Vorobyov, I.; Mackerell, A. D., Jr. CHARMM General Force Field: A Force Field for Drug-like Molecules Compatible with the CHARMM All-Atom Additive Biological Force Fields. *J. Comput. Chem.* **2010**, *31* (4), 671−690.
(36) Vermaas, J. V.; Petridis, L.; Ralph, J.; F Crowley, M.; T Beckham, G. Systematic Parameterization of Lignin for the CHARMM Force Field. *Green Chem.* **2019**, *21* (1), 109−122.
(37) Matthews, J. F.; Beckham, G. T.; Bergenstråhle-Wohlert, M.; Brady, J. W.; Himmel, M. E.; Crowley, M. F. Comparison of Cellulose Iβ Simulations with Three Carbohydrate Force Fields. *J. Chem. Theory Comput.* **2012**, *8* (2), 735−748.
(38) Guvench, O.; Hatcher, E.; Venable, R. M.; Pastor, R. W.; MacKerell, A. D., Jr. CHARMM Additive All-Atom Force Field for Glycosidic Linkages between Hexopyranoses. *J. Chem. Theory Comput.* **2009**, *5* (9), 2353−2370.
(39) Plazinska, A.; Plazinski, W. Comparison of Carbohydrate Force Fields in Molecular Dynamics Simulations of Protein−Carbohydrate Complexes. *J. Chem. Theory Comput.* **2021**, *17* (4), 2575−2585.
(40) Van Der Spoel, D.; Lindahl, E.; Hess, B.; Groenhof, G.; Mark, A. E.; Berendsen, H. J. C. GROMACS: Fast, Flexible, and Free. *J. Comput. Chem.* **2005**, *26* (16), 1701−1718.
(41) Huda, M. M.; Jahan, N.; Rai, N. Effect of Water Models on Structure and Dynamics of Lignin in Solution. *AIP Adv.* **2021**, *11* (6), No. 065024.
(42) Kirui, A.; Zhao, W.; Deligey, F.; Yang, H.; Kang, X.; Mentink-Vigier, F.; Wang, T. Carbohydrate-Aromatic Interface and Molecular Architecture of Lignocellulose. *Nat. Commun.* **2022**, *13* (1), No. 538.
(43) Kang, X.; Kirui, A.; Widanage, M. C. D.; Mentink-Vigier, F.; Cosgrove, D. J.; Wang, T. Lignin-Polysaccharide Interactions in Plant Secondary Cell Walls Revealed by Solid-State NMR. *Nat. Commun.* **2019**, *10* (1), No. 347.
(44) Vermaas, J. V.; Crowley, M. F.; Beckham, G. T. A Quantitative Molecular Atlas for Interactions Between Lignin and Cellulose. *ACS Sustainable Chem. Eng.* **2019**, *7* (24), 19570−19583.
(45) Vermaas, J. V.; Petridis, L.; Qi, X.; Schulz, R.; Lindner, B.; Smith, J.. C. Mechanism of Lignin Inhibition of Enzymatic Biomass Deconstruction. *Biotechnol. Biofuels* **2015**, *8* (1), No. 217.
(46) Čabalová, I.; Bélik, M.; Kučerová, V.; Jurczyková, T. Chemical and Morphological Composition of Norway Spruce Wood (Picea Abies, L.) in the Dependence of Its Storage. *Polymers* **2021**, *13* (10), No. 1619.
(47) Gindl, W.; Teischinger, A. Axial Compression Strength of Norway Spruce Related to Structural Variability and Lignin Content. *Composites, Part A* **2002**, *33* (12), 1623−1628.
(48) Kellogg, R. M.; Wangaard, F. F. Variation in The Cell-Wall Density of Wood. *Wood Fiber Sci.* **1969**, 180−204.
(49) Neagu, R. C.; Gamstedt, E. K.; Berthold, F. Stiffness Contribution of Various Wood Fibers to Composite Materials. *J. Compos. Mater.* **2006**, *40* (8), 663−699.
(50) Cave, I. D. The Anisotropic Elasticity of the Plant Cell Wall. *Wood Sci. Technol.* **1968**, *2* (4), 268−278.
(51) Cave, I. D. The Longitudinal Young's Modulus of Pinus Radiata. *Wood Sci. Technol.* **1969**, *3* (1), 40−48.
(52) Lin, K.-H.; Paterson, L.; May, F.; Andrienko, D. Glass Transition Temperature Prediction of Disordered Molecular Solids. *npj Comput. Mater.* **2021**, *7* (1), No. 179.
(53) Furuta, Y.; Aizawa, H.; Yano, H.; Norimoto, M. Thermal-Softening Properties of Water-Swollen Wood. IV. The Effects of Chemical Cconstituents of the Cell Wall on the Thermal-Softening Properties of Wood. *Mokuzai Gakkaishi* **1997**, *43* (9), 725−730.
(54) Kong, L.; Zhao, Z.; He, Z.; Yi, S. Effects of Steaming Treatment on Crystallinity and Glass Transition Temperature of Eucalyptuses grandis × E. Urophylla. *Results Phys.* **2017**, *7*, 914−919.
(55) Hasburgh, L. E.; Craft, S. T.; Van Zeeland, I.; Zelinka, S. L. Relative Humidity versus Moisture Content Relationship for Several Commercial Wood Species and Its Potential Effect on Flame Spread. *Fire Mater.* **2019**, *43* (4), 365−372.
(56) Glass, S. V.; Zelinka, S. L.; Johnson, J. A. *Investigation of Historic Equilibrium Moisture Content Data from the Forest Products Laboratory*; Forest Products Laboratory: 2014; 1−37. USDA Forest Service, Forest Products Laboratory, General Technical Report, FPL-GTR-229.

https://doi.org/10.1021/acsomega.3c08853
ACS Omega 2024, 9, 25646−25654

(57) Chen, P.; Wohlert, J.; Berglund, L.; Furó, I. Water as an Intrinsic Structural Element in Cellulose Fibril Aggregates. *J. Phys. Chem. Lett.* **2022**, *13* (24), 5424−5430.
(58) Kong, L.; Alqus, R.; Yong, C. W.; Todorov, I.; Eichhorn, S. J.; Bryce, R. A. Cellulose Iβ Microfibril Interaction with Pristine Graphene in Water: Effects of Amphiphilicity by Molecular Simulation. *J. Mol. Graphics Modell.* **2023**, *118*, No. 108336.
(59) Fredriksson, M.; Rüggeberg, M.; Nord-Larsen, T.; Beck, G.; Thybring, E. E. Water Sorption in Wood Cell Walls−Data Exploration of the Influential Physicochemical Characteristics. *Cellulose* **2023**, *30* (3), 1857−1871.

https://doi.org/10.1021/acsomega.3c08853
ACS Omega 2024, 9, 25646−25654